Influence of Droplet Spacing on Drag Coefficient in Nonevaporating, Monodisperse Streams

J. A. Mulholland*
U.S. Environmental Protection Agency, Research Triangle Park, North Carolina
R. K. Srivastava†
Acurex Corporation, Research Triangle Park, North Carolina
and
J. O. L. Wendt‡
University of Arizona, Tucson, Arizona

The influence of droplet spacing on the drag coefficient of individual drops injected into a quiescent environment has been determined through measurement of trajectories of single, monodisperse, nonevaporating droplet streams. Droplet size, velocity, and spacing were varied, yielding initial Reynolds numbers (Re) ranging from 90 to 290 and initial droplet spacing to diameter ratios (L/D) ranging from 1.7 to 1700. The effect of droplet spacing on the local drag coefficient C_D was of first-order importance but depended on Re. Data from 10 trajectories were correlated using asymptotic forms for C_D as follows: $[C_D(Re,L/D)]^{-n} = [C_D^0(Re,L/D)]^{-n} + [C_D^\infty(Re)]^{-n}$ where $C_D^0(Re,L/D) = C_D^0(Re) + aRe^{-1}[L/D - 1]$ and is the asymptotic form for C_D as $L/D \to 1$, whereas C_D^∞ is that for C_D as $L/D \to \infty$. A trajectory model containing the local drag coefficient was fitted to the experimental data by a nonlinear regression, yielding the following values for the empirical parameters: $n = 0.678$ and $a = 43.0$. The resulting model with this drag coefficient formulation was then able to predict over forty additional trajectories with acceptable accuracy. This formulation provides a first step for computing fuel and waste-droplet drag in flames, leading to improved predictions of combustion-generated air pollutants due to droplet penetration through flames.

Nomenclature

a_x = horizontal acceleration, m/s^2
a_y = vertical acceleration, m/s^2
a = parameter defined by Eq. (4)
A = area of droplet cross section [$=\pi D^2/4$], m^2
b = parameter defined by Eq. (2)
C_D = instantaneous drag coefficient on a droplet
C_D^0 = asymptotic form for C_D as $L/D \to 1$
C_D^∞ = drag coefficient for an isolated sphere
C_{rod} = friction drag coefficient for a long rod
D = droplet diameter, m
f = frequency of vibration, Hz
F_x = horizontal force [$=ma_x$], N
F_y = vertical force [$=ma_y$], N
g = acceleration to gravity, m/s^2
L = distance between centers of two droplet neighbors, m
L^0 = initial distance between droplet [$=L_sN$], m
L_s = distance between droplets of unseparated droplet stream, m
m = droplet mass, kg
n = parameter defined by Eq. (5)
N = number of frequency divisions
p = horizontal velocity [$=dx/dt$], m/s
q = vertical velocity [$=dy/dt$], m/s
$\dot{q}$ = flow rate of droplet stream, ℓ/s
Re = Reynolds number [$=\rho_d VD/\mu_a$]
Re^0 = initial Reynolds number
t = time, s
V = magnitude of droplet velocity [$=(p^2+q^2)^{1/2}$], m/s
V^0 = initial droplet velocity, m/s
x = horizontal coordinate, m
y = vertical coordinate, m
ρ_a = density of air, kg/m^3
ρ_d = density of droplet, kg/m^3
θ = angle between trajectory and horizontal axis

Introduction

IT is well established that droplet interactions profoundly influence the ignition and combustion behavior of droplet clouds and fuel sprays.[1,2] Four group combustion modes of a droplet cloud have been identified,[1] with that of single-droplet combustion possibly being applicable in practice to only a very limited number of special situations.[3] Such a special situation, however, can arise during the incineration of liquid hazardous wastes, where droplets with large diameters congregate at the outer edge of fuel spray cones.[4,5] One or more of these stray droplets then may individually pass through, or bypass, the main flame zone and lead to a failure mode in the incinerator. For example, bypassing of as few as one drop out of 10 million can lead to failure to meet a destruction removal efficiency (DRE) in excess of 99.99%, as is required by law. Even if DRE requirements are met, incomplete combustion of large droplets can result in increased emissions of products of incomplete combustion.

Motivation for the current study lay, therefore, in the need to predict single-droplet passage through a turbulent flame zone and the resulting trajectory in an incinerator firebox. To this end, experiments have been conducted 1) to measure the trajectories of single, monodisperse droplet streams in hot, swirling combustion flowfields, as functions of the droplet

Received March 9, 1987; revision received Feb. 29, 1988.

*Mechanical Engineer, Combustion Research Branch, Air and Energy Engineering Research Laboratory; currently Graduate Student, Department of Chemical Engineering, Massachusetts Institute of Technology, Cambridge, Massachusetts.
†Mechanical Engineer, Southeast Regional Office.
‡Professor, Department of Chemical Engineering.

injection parameters of size, velocity, spacing, and angle, and 2) to correlate droplet penetration with droplet incineration. Preliminary results[6,7] indicated that 1) droplet penetration could change by over a factor of three, with only the initial spacing between drops being varied, and 2) increased droplet penetration can result in failure to achieve 99.99% DRE. To predict these results, a general three-dimensional algorithm for modeling droplet trajectories in hot combustor flowfields is under development. One of the inputs to this model is a proper representation of the drag on a droplet during initial heating and evaporation. Although much data are available on the relationship of the drag coefficient C_D of an isolated, nonevaporating sphere to Reynolds number Re, little information is available on the dependence of C_D on droplet spacing, nondimensionalized by droplet diameter D as L/D. Droplets in streams that are aligned in tandem along the direction of relative motion with the gas stream experience a reduced drag due to wake effects. The objective of this paper, therefore, is to quantify the dependence of C_D on both Re and L/D, with a view toward establishing a functional relationship that can be used as input into the final droplet trajectory model.

It is recognized that the effect of droplet spacing on penetration of a monodisperse stream into a combustor can be attributed to a combination of at least three phenomena. First, ignition delay times increase by nearly fourfold as the spacing is made very small;[8] second, the combustion rate is decreased;[9] and third, the drag coefficient is decreased, as just described. Quantification of this last effect, recognized by Sangiovanni and Kesten,[8] is the sole focus of the work reported in this paper. Further, it is recognized that evaporation reduces drag by as much as 70%.[10] This paper considers only the case of a nonevaporating droplet. Finally, the reader is reminded that the influence of droplet spacing on drag coefficient described in this paper is limited to the case of a tandem alignment of droplets; the effect is reduced for adjacent droplets aligned at an angle to the direction of relative motion.

Theory

Drag Coefficient

When droplets cease to interact, the drag coefficient C_D^∞ for each one is that of an isolated sphere ($L/D \to \infty$). The conventional correlation for the drag on a solid sphere in steady motion typically is presented as a plot denoted as the "standard drag curve," where C_D^∞ is plotted as a function of Re.[11] Many empirical or semi-empirical equations have been used to approximate this curve. For $Re < 800$, Schiller and Naumann found a correlation involving the Stokes Law relation multiplied by a Re correction term.[12]

$$C_D^\infty(Re) = (24/Re)(1 + 0.15Re^{0.687}) \tag{1}$$

Liquid droplets behave differently than hard spheres due to distortion, internal fluid circulation, and evaporation. These effects can significantly reduce drag in highly accelerated[13] and evaporating[10] droplets. However, for low-velocity droplets in a quiescent environment, the Schiller and Naumann expression can be modified slightly to provide a good first-order approximation for isolated droplet drag.

$$C_D^\infty(Re) = (24/Re)(1 + bRe^{0.687}) \tag{2}$$

The parameter b is determined from experimental data.

In the other extreme, as droplet spacing approaches the droplet diameter ($L/D \to 1$), the drag coefficient may be assumed to approach the friction drag coefficient of a long rod C_{rod}. For very long rods, the theory of Glauert and Lighthill[14] yields[15]

$$C_{\text{rod}}(Re) = 0.755/Re \tag{3}$$

A general form for the drag coefficient of a sphere as L/D approaches unity C_D^0 is obtained by a Taylor expansion about $L/D = 1$; thus, C_D^0 is hypothesized to be

$$C_D^0(Re, L/D) = C_D^{0'}(Re) + aRe^{-1}(L/D - 1) \tag{4}$$

where C_D^0 is related to C_{rod} by Eq. (6), and a is a parameter to be determined from experiment.

The factor (aRe^{-1}) multiplying $(L/D - 1)$ in Eq. (4) is assumed to be a function of Re because the extent to which droplet spacing influences the local drag coefficient depends on the length of wake behind each droplet.[16] Fornberg[17] has calculated the wake length behind a cylinder for a range of Reynolds numbers up to 300. He found that wake length increases approximately linearly with Re, growing from 1 to 40 diameters as Re increases from 2 to 260. Above $Re = 260$, the wake region ceases to increase but becomes slightly shorter and wider. These results are relevant to this problem because, even though the drag coefficient of an isolated sphere is about half that for an isolated cylinder, the dependence of C_D on Re is similar. Therefore, it is assumed that the dependence of wake length on Re is also similar. Hence, the linear dependence of wake length on Re suggests that the exponent on Re in Eq. (4) should be approximately equal to -1.

Following Churchill[18] and Churchill and Usagi,[19] an effective and universal technique to correlate data, obtained between regions of validity for the asymptotic forms for C_D as $L/D \to 1$ and $L/D \to \infty$, is to use the following expression for C_D, valid for all values of L/D:

$$[C_D(Re, L/D)]^{-n} = [C_D^0(Re, L/D)]^{-n} + [C_D^\infty(Re)]^{-n} \tag{5}$$

where n is a parameter to be obtained by experiment. From Eqs. (3-5), it follows that at $L/D = 1$

$$[C_D^{0'}(Re)]^{-n} = [C_{\text{rod}}(Re)]^{-n} - [C_D^\infty(Re)]^{-n} \tag{6}$$

Equation (5), therefore, represents an expression for the drag coefficient C_D of a droplet where the asymptotic limits C_D^∞ and C_D^0 are given by Eqs. (2) and (4).

The model as has been described contains three unknown parameters: a, b, and n. Parameter b represents an adjustment to the hard-sphere drag coefficient correlation for isolated liquid droplets; parameters a and n represent the dependence of C_D on droplet spacing. In this work, the parameters a, b, and n are determined entirely from experimental data. However, for $Re > 250$, where the wake length may be considered to be roughly constant,[17] only a few data points were collected, making it impossible to confirm that the limiting droplet separation, at which interactions cease to be important, is also independent of Re. Therefore, this hypothesis is assumed to be true, and a discontinuity in the model is introduced to ensure that for $Re > 250$, the value of L/D, at which $C_D = 0.95\, C_D^\infty$, no longer depends on Re. Thus, the model of the effect of droplet spacing on the local drag coefficient is consistent with available calculations on the effect of Re on wake length behind a cylinder.

Trajectory Model

A simple force balance comprises the model to predict droplet trajectories in a quiescent environment:

$$\Sigma_{F_x} = ma_x = -C_D(\rho_a V^2 A/2)\cos\theta \tag{7}$$

$$\Sigma_{F_y} = ma_y = -C_D(\rho_a V^2 A/2)\sin\theta - mg \tag{8}$$

These equations yield

$$\frac{dx}{dt} = p \tag{9}$$

$$\frac{dp}{dt} = -\frac{3\rho_a}{4\rho_d D} C_D p(p^2 + q^2)^{1/2} \tag{10}$$

$$\frac{dy}{dt} = q \tag{11}$$

$$\frac{dq}{dt} = -\frac{3\rho_a}{4\rho_d D} C_D q(p^2 + q^2)^{1/2} - g \tag{12}$$

with

$$x(0) = 0, \quad y(0) = 0, \quad p(0) = V^0, \quad q(0) = 0 \tag{13}$$

Complexities arise in that C_D [Eq. (5)] is a function of Re and L/D, both of which are continuously changing in the Lagrangian frame of reference. For nonevaporating droplets produced at a steady rate, conservation of mass yields

$$L(t) = L^0 V(t)/V^0 \tag{14}$$

where $V = (p^2 + q^2)^{1/2}$. Thus, instantaneous values of droplet spacing and, subsequently, instantaneous values of C_D (Re,L/D) can be computed. Droplet spacing and velocity are very sensitive to local conditions. Equation (14) is valid for idealized initial conditions and the absence of flow disturbances. For given values of a, b, and n, Eqs. (9–12) were numerically integrated to yield $x(t)$, $y(t)$, and $V(t)$, using Eqs. (2), (4), (5), and (14) to evaluate C_D.

Experimental Methods

Apparatus

The droplet generator is a vibrating orifice device with ancillary electronics to facilitate droplet spacing variation[20,21] (Fig. 1). The longitudinally vibrating orifice, driven by a signal generator at about 13 kHz, reinforces the natural Rayleigh instability of the liquid jet, thereby producing a monodisperse stream of droplets without satellites. To vary droplet spacing, droplets are charged periodically by a pulsed charging ring and then deflected by parallel high-voltage plates. The neutral droplets are trapped and recirculated, while the charged droplets enter a closed trajectory observation tunnel where fluctuating air currents are minimized.

Two fluids, chosen on the basis of conductivity (for electrostatic charging and deflection) and viscosity (for droplet formation), were tested. The first, a mixture of 80% (by volume) Shell Oil Company fuel additive ASA-3, comprised mostly of xylene (C_8H_{10}), and 20% distillate fuel oil, was used for its applicability to combustion fuel atomization studies; the second, a mixture of water (H_2O) and glycerine ($C_3H_8O_3$), was used for comparison. Droplet parameters varied were spacing, size, and velocity. Spacing, nondimensionalized as L/D, was varied by adjusting the frequency divider setting N, which controls the charging ring pulse rate. Size D was varied by changing orifice sizes, with droplet diameters found to be approximately twice the orifice diameter. Droplet velocity V was varied by adjusting the liquid supply pressure and, hence, the liquid flow rate. Droplet spacing was varied independently of other variables, whereas droplet size and velocity variations were not independent.

Relative values of droplet diameter and droplet spacing L_s in the uncharged stream were measured using a stroboscope to freeze droplet motion and a microscope to magnify the droplet images. Droplet size and spacing were observed stroboscopically under a microscope over long periods of time and were found to be constant to within the measurement limitations of the apparatus (within $\pm 10\,\mu$m). Absolute droplet diameter was calculated from measurements of volumetric flow rate $\dot{q}$ and vibrator frequency f. Conservation of mass yields

$$D = (6\dot{q}/\pi f)^{1/3} \tag{15}$$

The initial droplet spacing after separation L^0 is given by

$$L^0 = L_s N \tag{16}$$

Initial droplet velocity V^0 is given by

$$V^0 = L_s f \tag{17}$$

Droplet trajectories were measured by manually recording two-dimensional coordinates from droplet shadows on graph paper. The trajectory starting point was defined at the center of the deflection plates, where the droplet path was horizontal as determined by a level gage.

Qualitative verification of Eqs. (14–17) was achieved by photographing droplet streams at various magnifications and by microscopic scrutiny. Fluctuations in initial droplet size and velocity were less than 5% of the mean. Evaporation during droplet flight did not occur to a significant extent (less than 10%). Although small fluctuations in initial conditions and slight droplet vaporization may account for some discrepancies between experiment and model, these nonidealities are minor. Thus, the measurement techniques used here, consistent with those used by Choi and Churchill[22] in similar experiments on burning droplets, are valid for obtaining first-order effects of droplet spacing on drag coefficient in nonevaporating, monodisperse streams.

Approach

Experimental measurements consisted of full trajectories and trajectory endpoints. Full trajectories contained between a minimum of six and a maximum of 15 x-y coordinate pairs describing the complete trajectory of a droplet from the injection point to an endpoint that lay between 11.7 and 14.8 cm below. Trajectory endpoints, on the other hand, consisted merely of the horizontal distance traveled for a given vertical height ranging from 7 to 14 cm.

The experiments were conducted in three parts. First, an isolated droplet drag coefficient C_D^∞ was measured, and parameter b in Eq. (2) was evaluated. Second, parameters a and n were estimated by nonlinear regression of data for 10 full trajectories (nos. 1–10 on Table 1). Initial Reynolds number Re^0 was 211, and initial droplet spacing to diameter ratio L^0/D was varied from 2.7 to 1365 ($1 \le N \le 512$). Note, however, that local values of both Re and L/D changed dramatically during the course of each single trajectory, thus allowing a Re dependence to be determined. Third, four additional full trajectories (nos. 11–14 on Table 1) yielded data at different initial Reynolds numbers. These were compared to model predictions. A total of 39 trajectory endpoints on Table 2, spanning a wider range of parameters ($90 < Re^0 < 292$, $6.7 < V^0 < 9.9$ m/s, $205 < D < 450\,\mu$m, $2.4 < L^0/D < 1500$), completed the comparison between prediction and experiment.

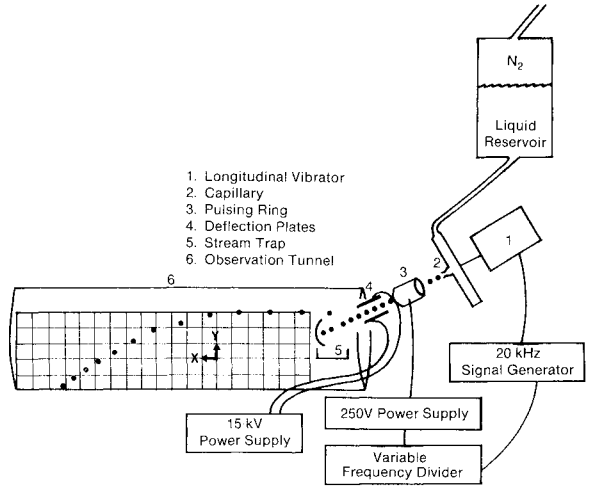

Fig. 1 Monodisperse droplet generator with ancillary electronics and two-dimensional trajectory measurement apparatus.

Table 1 Full trajectory data

Trajectory[a]	X(cm)	Y(cm)
#1	5.0	0.0
$D = 324$ μm	8.5	−0.13
$V^0 = 10.02$ m/s	18.7	−0.13
$Re^0 = 211$	28.8	−0.25
$L^0/D = 2.67$	39.0	−0.38
	54.2	−0.89
	69.5	−2.03
	84.7	−3.81
	99.9	−6.35
	122.8	−11.7
#2	5.0	0.0
$D = 324$ μm	8.5	−0.13
$V^0 = 10.02$ m/s	18.7	−0.25
$Re^0 = 211$	28.8	−0.38
$L^0/D = 5.33$	39.0	−0.64
	54.2	−1.52
	69.5	−2.79
	84.7	−6.60
	105.0	−11.7
#3	5.0	0.0
$D = 324$ μm	8.5	−0.13
$V^0 = 10.02$ m/s	18.7	−0.25
$Re^0 = 211$	28.8	−0.38
$L^0/D = 10.7$	39.0	−0.64
	54.2	−1.78
	69.5	−4.06
	87.2	−11.7
#4	5.0	0.0
$D = 324$ μm	8.5	−0.13
$V^0 = 10.02$ m/s	18.7	−0.25
$Re^0 = 211$	28.8	−0.51
$L^0/D = 21.3$	39.0	−0.76
	54.2	−2.29
	69.5	−4.57
	84.7	−11.7
#5	5.0	0.0
$D = 324$ μm	8.5	−0.13
$V^0 = 10.02$ m/s	18.7	−0.25
$Re^0 = 211$	28.8	−0.64
$L^0/D = 42.6$	39.0	−0.89
	54.2	−2.29
	69.5	−5.84
	82.2	−11.7
#6	5.0	0.0
$D = 324$ μm	8.5	−0.13
$V^0 = 10.02$ m/s	18.7	−0.51
$Re^0 = 211$	28.8	−0.76
$L^0/D = 85.3$	39.0	−1.27
	54.2	−2.54
	77.1	−11.7
#7	5.0	0.0
$D = 324$ μm	8.5	−0.13
$V^0 = 10.02$ m/s	18.7	−0.51
$Re^0 = 211$	28.8	−0.76
$L^0/D = 171$	39.0	−1.52
	54.2	−4.06
	72.2	−11.7
#8	5.0	0.0
$D = 324$ μm	8.5	−0.13
$V^0 = 10.02$ m/s	18.7	−0.51
$Re^0 = 211$	28.8	−0.76
$L^0/D = 341$	39.0	−2.03
	54.2	−4.57
	68.2	−11.7
#9	5.0	0.0
$D = 324$ μm	8.5	−0.13
$V^0 = 10.02$ m/s	18.7	−0.51
$Re^0 = 211$	28.8	−0.76
$L^0/D = 682$	39.0	−1.52
	68.2	−11.7
#10	5.0	0.0
$D = 324$ μm	8.5	−0.13
$V^0 = 10.02$ m/s	18.7	−0.51
$Re^0 = 211$	28.8	−1.02
$L^0/D = 1365$	39.0	−1.78
	69.5	−11.7
#11	5.0	0.0
$D = 234$ μm	7.5	−0.05
$V^0 = 7.72$ m/s	17.5	−0.29
$Re^0 = 117$	28.0	−0.54
$L^0/D = 2.54$	38.0	−1.3
	48.0	−2.1
	58.0	−2.8
	69.0	−4.6
	79.0	−6.7
	89.0	−7.9
	99.0	−11.0
	104.0	−14.8
	109.0	−13.5
#12	5.0	0.0
$D = 234$ μm	13.0	−0.16
$V^0 = 7.72$ m/s	18.0	−0.32
$Re^0 = 117$	28.0	−0.95
$L^0/D = 162$	39.0	−2.9
	49.0	−7.9
	55.0	−13.0
#13	5.0	0.0
$D = 450$ μm	7.5	−0.05
$V^0 = 9.95$ m/s	17.5	−0.29
$Re^0 = 292$	28.0	−0.54
$L^0/D = 1.70$	38.0	−1.05
	48.0	−1.3
	58.0	−2.06
	69.0	−2.09
	79.0	−3.19
	89.0	−4.86
	99.0	−6.2
	109.0	−7.65
	119.0	−9.7
	129.0	−12.0
	135.0	−14.8
#14	5.0	0.0
$D = 450$ μm	9.0	−0.3
$V^0 = 9.95$ m/s	19.0	−0.5
$Re^0 = 292$	29.0	−0.6
$L^0/D = 109$	39.0	−1.3
	49.0	−2.3
	60.0	−3.6
	70.0	−5.8
	95.0	−14.0

[a]Trajectories 1-10 with 80% C_8H_{10}/20% no. 2 fuel oil droplet; trajectories 11-14 with 75% H_2O/25% $C_3H_8O_3$ droplet.

Experimental Results

Data from full trajectory and trajectory endpoint measurements are presented in Tables 1 and 2, respectively. Accuracy of trajectory coordinates was estimated to be ±0.2 cm. In addition, some data scatter was observed, approximating a ±2-cm variation in the horizontal position at the trajectory endpoint.

Isolated Droplets

Parameter b was estimated using data from trajectories of streams with large initial droplet spacing. Trajectories 8, 9, and 10 in Table 1 are nearly identical, indicating that droplet interactions are insignificant in streams with $L^0/D > 340$. From these data, a value of b of 0.11 was derived. This value results in an isolated droplet drag coefficient [Eq. (2)] of slightly less than the hard-sphere drag coefficient of Schiller and Naumann[12] [Eq. (1)]. Figure 2 depicts this result, with Ingebo's results[13] from high-velocity droplet streams shown for comparison. As a first-order approximation, the hard-sphere model could be used to describe the isolated droplet drag observed in this study. For remainder of this analysis, however, the modified drag coefficient asymptote C_D^∞, given by Eq. (2) with $b = 0.11$ and represented by curve 3 in Fig. 2, is used.

Droplet Streams

Parameters a and n were estimated using data from the first 10 trajectories of Table 1. Nonlinear regression for parameter estimation was achieved using a modified Marquardt[23] algorithm based on a multidimensional search in parameter space for the minimum value of a sum of squares functional measuring deviation from the data. A special feature of the algorithm calculates the sensitivity matrix $(\partial F_i/\partial\theta_j)$ relating the change in the ith predicted value F_i with each parameter θ_j. This quantity indicates which parameters contribute first-order and second-order effects. For example, sensitivity analysis indicated that a is the least sensitive parameter in the drag coefficient formulation; hence, one would expect rather wide confidence limits on this parameter.

The least-squares parameter estimated, obtained with both parameters placed in regression, and the approximate 95% confidence limits are

$$a = 43.0 \pm 15.4$$

$$n = 0.678 \pm 0.07$$

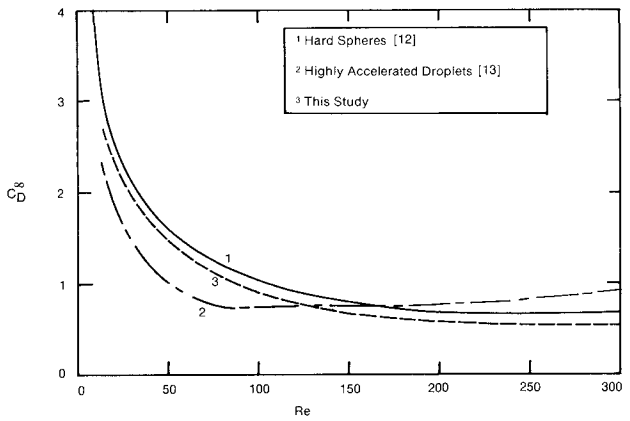

Fig. 2 Isolated droplet drag coefficient as a function of *Re*.

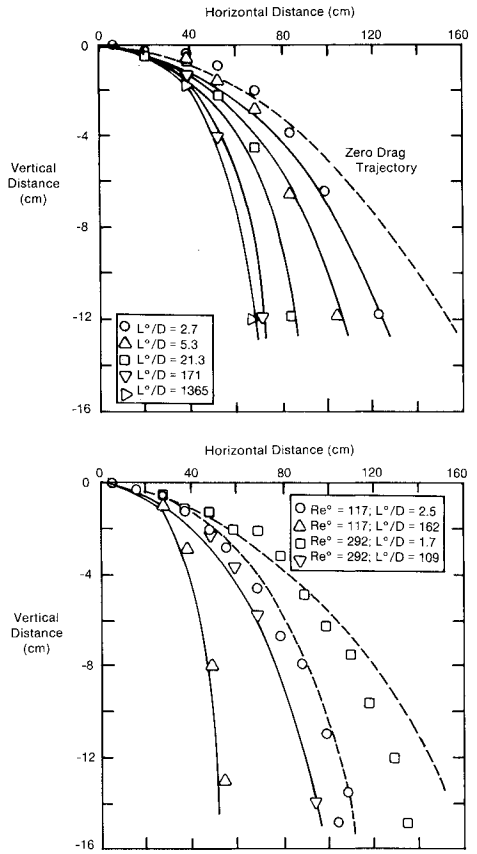

Fig. 3 Two-dimensional droplet trajectories. Points represent measured trajectories; lines are model results. Results of five trajectories from the best-fit nonlinear regression of 10 full trajectories at $Re^0 = 211$ are shown in the top plot. Model predictions of four more full trajectories are shown in the bottom plot. Solid lines represent $Re^0 = 117$ predictions; dashed lines represent $Re^0 = 292$ predictions.

The confidence limits on parameter a reflect the confidence on the initial slope of C_D as $L/D \rightarrow 1$, whereas those on parameter n reflect the confidence on the curvature of C_D as $C_D \rightarrow C_D^\infty$. Sensitivity analysis indicates very low sensitivity of the C_D parameters during the initial portion of a droplet trajectory. The parameters are most sensitive at the trajectory endpoints. Therefore, prediction of trajectory endpoints is a severe test of the C_D formulation and trajectory model.

Other statistical quantities that measured model adequacy were determined as $R^2 = 0.990$ (model effectiveness) and F-test = 0.04 (percent probability that model is not an improvement over no model at all).

Table 2 Single-point trajectory data

	L^0/D	Height (cm)	Range (cm)
Fluid 1[a]	2.52	8.89	61
$D = 205$ μm	5.04	8.57	51
$V^0 = 6.71$ m/s	10.1		43
$Re^0 = 89.6$	20.2		37
	40.3		33
	80.7		32
	161		28
	323		28
	646		27
	1291		27
Fluid 2[b]	2.40	7.30	76
$D = 225$ μm	4.80		71
$V^0 = 7.02$ m/s	9.60		63
$Re^0 = 110$	19.2		56
	38.4		53
	76.8		50
	154		48
	307		48
	614		48
	1229		47
Fluid 2[b]	2.92	7.30	86
$D = 234$ μm	5.85		84
$V^0 = 8.89$ m/s	11.7		76
$Re^0 = 136$	23.4		66
	46.8		61.5
	93.5		61
	187		54.5
	374		54.5
	748		54.5
	1497		54.5
Fluid 3[c]	3.40	13.97	118
$D = 450$ μm	6.80		115
$V^0 = 9.94$ m/s	13.6		110
$Re^0 = 292$	27.2		103
	54.4		100
	109		95
	218		94
	435		91
	870		91

[a]Fluid 1: 80% C_8H_{10}/20% no. 2 fuel oil.
[b]Fluid 2: 50% H_2O/50% $C_3H_8O_3$.
[c]Fluid 3: 75% H_2O/25% $C_3H_8O_3$.

Predictions

Model predictions are compared to experimental measurements in Fig. 3 (full trajectories) and Fig. 4 (trajectory endpoints). The upper portion of Fig. 3 shows the model fit to five of the 10 trajectories used in the regression analysis. The experimental data shown cover the entire range of trajectories for various droplet spacings. The dashed line corresponds to the hypothetical limit of zero drag whereas, at the other extreme, the solid line for $L^0/D = 1365$ represents the limit for isolated spheres. Droplet interactions lead to trajectories lying between these extremes and, clearly, are of first-order importance. The remaining four trajectories (Fig. 3, lower portion) are predicted reasonably well. The largest discrepancy arises at high initial Reynolds number ($Re^0 = 292$) and close initial spacing ($L^0/D = 1.70$), when droplets penetrated almost to the end of the observation tube where the quiescent environment may have been disturbed.

The upper portion of Fig. 4, depicting measured and predicted trajectory endpoints for all 10 trajectories included in regression, clearly shows the importance of droplet spacing in determining droplet penetration at a constant initial Reynolds number ($Re^0 = 211$). As initial droplet spacing is reduced below $L^0/D = 150$ [$\ell n(L^0/D) = 5$], a significant drag reduction greatly increases the horizontal range for a fixed 11.7-cm vertical drop.

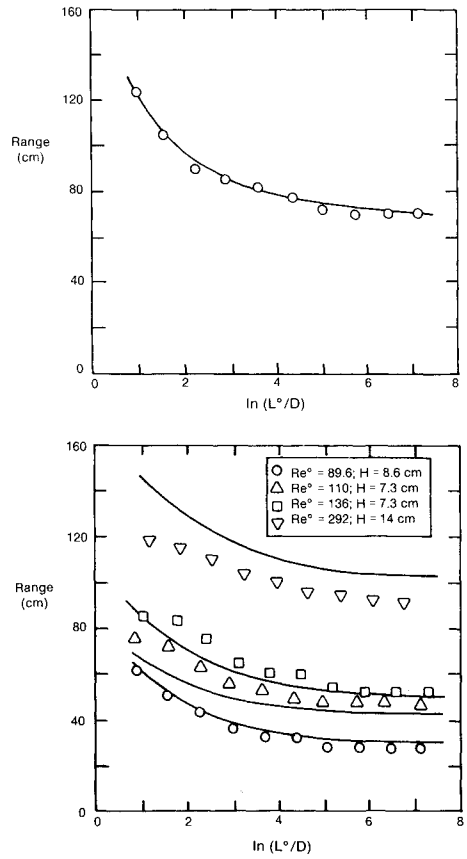

Fig. 4 Droplet trajectory endpoints. Points represent measured trajectory endpoints; lines are model results. Results from the best-fit nonlinear regression of 10 full trajectories at $Re^0 = 211$, with the endpoint being the horizontal distance (range) that a droplet travels while falling a vertical distance H of 11.7 cm, are shown in the top plot. Model predictions of 39 more trajectory endpoints are shown in the bottom plot.

The lower portion of Fig. 4 shows model predictions for 39 trajectory endpoints, grouped into four sets. Each set corresponds to a different Re^0, as shown. Good agreement was achieved, with one exception. For the high Re^0 condition, the model overpredicted the range of the closely spaced droplets. As discussed above, this discrepancy may be due to perturbations in the quiescent environment for droplets penetrating too close to the end of the observation tube.

Discussion

The influence of droplet spacing on the drag coefficient for various Reynolds numbers is shown in Fig. 5. The intersection of the vertical axis is given by C_{rod}, which has a very low value. Each curve asymptotically approaches C_D^∞, although at high Reynolds numbers this approach appears to be surprisingly slow. Since data in Fig. 4 suggest that spacing has little practical effect on penetration when $L^0/D > 150$, it might be argued that the very slow final approach to the C_D^∞ asymptote is an artifact of our formulation [Eq. (5)], and that it leads to negligible error in practice. For $L^0/D < 150$, however, it is clear that droplet spacing has a first-order effect on the drag coefficient, which can be significantly diminished through aerodynamic interactions with the droplet neighbors.

The confidence limits on the individual drag coefficient parameters can be propagated to yield confidence limits on C_D using a procedure for correlated, multivariable problems. Results of this calculation for $Re = 25$ are shown by the shaded region in Fig. 5. The approximated 95% confidence interval on C_D for this formulation as a function of Re and L/D is a crude indication of the accuracy (and uncertainty) with which C_D has

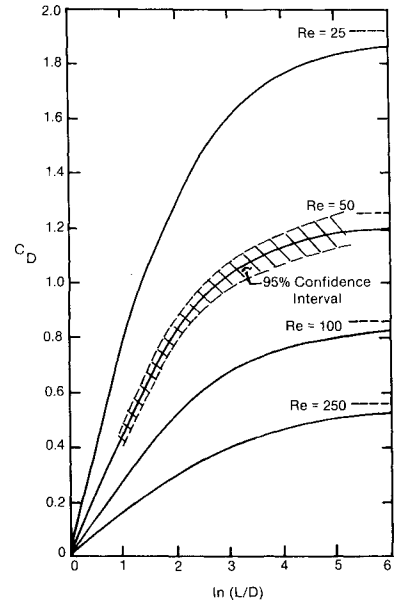

Fig. 5 Droplet drag coefficient as a function of Re and L/D. The dashed lines on the right axis indicate the value of the drag coefficient of an isolated droplet at each Re value plotted.

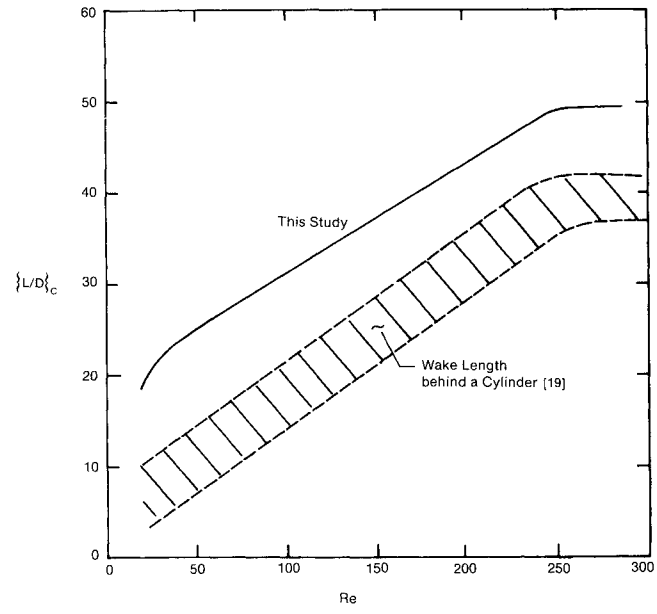

Fig. 6 Critical droplet spacing as a function of Re, for a C_D value of 80% of that of an isolated droplet. The shaded region represents the numerical solution of Fornberg[17] for the wake length behind a circular cylinder.

been defined. Figure 5 shows that, despite the relatively large 95% confidence interval on parameter a ($\pm 36\%$), the uncertainty in C_D is small (less than 10%).

It is useful to define a critical droplet spacing $[L/D]_C$, above which no significant effect on drag coefficient is observed. This critical droplet spacing should be related to the wake length behind a sphere. Therefore, it is expected that this parameter should have a similar dependence on Reynolds number as wake length. In Fig. 6 the numerical calculation of wake length behind a circular cylinder by Fornberg[17] is shown. The experimental results represent critical droplet spacing as a function of Reynolds number defined by a drag coefficient of 80% of C_D^∞. The choice of this definition is arbitrary, but it would be convenient to have critical droplet spacing be of the same order as Fornberg's wake lengh. Figure 6 illustrates the similarity in

Reynolds number dependence between Fornberg's calculations and this paper's empirical drag formulation. Critical droplet spacing is nearly linear with Reynolds number for $Re \leq 250$.

Note that, even though the three-parameter formulation of C_D, as a function of Re and L/D, predicted two-dimensional trajectories very well (provided $Re^0 < 250$) over the entire range of droplet spacings, it may not be the only valid formulation. Other models may work as well. Indeed, it would be desirable to replace the empiricism in this paper with a more mechanistic approach, e.g., that of Fornberg.[17]

In conclusion, the drag coefficient of a nonevaporating monodisperse droplet stream has been found to be a function of both Reynolds number and droplet spacing. An empirical model for drag coefficient computation has been proposed. This model is being upgraded for three-dimensional use and incorporated into a droplet trajectory flame code for evaluating the phenomena of droplets bypassing and penetrating the flame zone. Applications of this modeling tool can be used to predict hazardous waste incinerator failure modes and combustion pollutant emissions.

Acknowledgments

This research was conducted in the U.S. Environmental Protection Agency's Air and Energy Engineering Research Laboratory (AEERL) at Research Triangle Park, North Carolina. Financial support was provided by EPA's Hazardous Waste Engineering Research Laboratory (HWERL). The authors are grateful to J. V. Ryan and J. VanRoy of Acurex Corporation for their assistance in completing the experiments. The authors also acknowledge the support of Robert E. Hall, Chief of EPA's Combustion Research Branch. One author (J. O. L. Wendt) is grateful to the National Research Council for their support during his tenure as NAS/NAE Senior Visiting Scientist at EPA.

References

[1]Chiu, H. H., Kim, H. Y., and Croke, E. J., "Internal Group Combustion of Liquid Droplets," *Nineteenth Symposium (International) on Combustion,* The Combustion Institute, Pittsburgh, PA, 1983, pp. 971–980.

[2]Chigier, N. A. and McCreath, C. G., "Combustion of Droplets in Sprays," *Acta Astronautica,* Vol. 1, May–June 1974, pp. 687–710.

[3]Chigier, N. A., "Instrumentation Techniques for Studying Heterogeneous Combustion," *Progress in Energy and Combustion Science,* Vol. 3, No. 3, 1977, pp. 175–189.

[4]Kramlich, J. C., Heap, M. P., Seeker, W. R., and Samuelsen, G. S., "Influence of Atomization Quality on the Destruction of Hazardous Waste Compounds," *Twenty-First Symposium (International) on Combustion,* The Combustion Institute, Pittsburgh, PA, 1988, pp. 593–600.

[5]Kramlich, J. C., Heap, M. P., Seeker, W. R., and Samuelsen, G. S., "Flame-Mode Destruction of Hazardous Waste Compounds," *Twentieth Symposium (International) on Combustion,* The Combustion Institute, Pittsburgh, PA, 1985, pp. 1991–1999.

[6]Mulholland, J. A., Srivastava, R. K., and Ryan, J. V., "The Role of Rogue Droplet Combustion in Hazardous Waste Incineration," *Proceedings of the Twelfth Annual Research Symposium on Land Disposal, Remedial Action, Incineration and Treatment of Hazardous Wastes,* Environmental Protection Agency, Washington, DC, EPA/600/9-86/022 (NTIS PB87-119491), 1986, pp. 413–420.

[7]Mulholland, J. A., Srivastava, R. K., and Ryan, J. V., "Influence of Rogue Droplet Atomization on Incineration Effectiveness," The Combustion Institute, Pittsburgh, PA, Paper WSS-86-23, Oct. 1986.

[8]Sangiovanni, J. J. and Kesten, A. S., "Effect of Droplet Interaction on Ignition in Monodispersed Droplet Streams," *Sixteenth Symposium (International) on Combustion,* The Combustion Institute, Pittsburgh, PA, 1977, pp. 577–592.

[9]Koshland, C. P. and Bowman, C. T., "Combustion of Monodisperse Droplet Clouds in a Reactive Environment," *Twentieth Symposium (International) on Combustion,* The Combustion Institute, Pittsburgh, PA, 1985, pp. 1799–1807.

[10]Eisenklam, P., Arunachalam, S. A., and Weston, J. A., "Evaporation Rates and Drag Resistance of Burning Drops," *Eleventh Symposium (International) on Combustion,* The Combustion Institute, Pittsburgh, PA, 1967, pp. 715–728.

[11]Schlichting, H., *Boundary Layer Theory,* 7th ed., McGraw-Hill, New York, 1979, p. 17.

[12]Clift, R., Grace, J. R., and Weber, M. E., *Bubbles, Drops, and Particles,* Academic Press, New York, 1978, p. 111.

[13]Ingebo, R. D., "Atomization, Acceleration, and Vaporization of Liquid Fuels," *Sixth Symposium (International) on Combustion,* Reinhold, New York, 1957, pp. 684–687.

[14]Glauert, M. B. and Lighthill, M. J., "The Axisymmetric Boundary Layer on a Long Thin Cylinder," *Proceedings of the Royal Society of London,* Ser. A., Vol. 230, 1955, pp. 188–203.

[15]White, F. M., *Viscous Fluid Flow,* McGraw-Hill, New York, 1974, pp. 349–350.

[16]Panton, R. L., *Incompressible Flow,* 1st ed., Wiley, New York, 1984, pp. 384–401.

[17]Fornberg, B., "A Numerical Study of Steady Viscous Flow Past a Circular Cylinder," *Journal of Fluid Mechanics,* Vol. 98, Pt. 4, June 1980, pp. 819–855.

[18]Churchill, S. W., *The Interpretation and Use of Rate Data: The Rate Concept,* McGraw-Hill, New York, 1974, Chap. 10, pp. 290–296.

[19]Churchill, S. W. and Usagi, R., "General Expression for the Correlation of Rates of Transfer and Other Phenomena," *American Institute of Chemical Engineers Journal,* Vol. 18, No. 6, 1972, pp. 1121–1128.

[20]Seymour, R. J. and Boss, C. B., "Design Modification for a Uniform Droplet Generator System," *Applied Spectroscopy,* Vol. 37, No. 4, 1983, pp. 375–379.

[21]Russo, R. E., Withnell, R., and Hieftje, G. M., "Simple and Inexpensive Design for an Isolated Droplet Generator Useful in Studies of Atomization in Flames," *Applied Spectroscopy,* Vol. 35, No. 6, 1981, pp. 531–536.

[22]Choi, B. and Churchill, S. W., "Evaporation and Combustion of Uniformly Sized Hexane Droplets in a Refractory Tube," *Advances in Chemistry Series,* No. 166, 1978, pp. 83–92.

[23]Marquardt, D. L., "An Algorithm for Least-Squares Estimation of Non-Linear Parameters," *Journal of the Society of Industrial and Applied Mathematics,* Vol. 11, No. 2, June 1963, pp. 431–441.